IARJSET ISSN (O) 2393-8021, ISSN (P) 2394-1588

International Advanced Research Journal in Science, Engineering and Technology

Impact Factor 8.311 ⁜ Peer-reviewed & Refereed journal ⁜ Vol. 13, Issue 10, October 2026

DOI: 10.17148/IARJSET.2026.131039

Fe-Induced Modulation of Structural, AC Conductivity and Dielectric Properties of ZnO Nanostructures

Dr. Anil Kaushik

Assistant Professor of Physics, GCW Gohana, Sonepat, Haryana, India

Abstract: Fe-modified ZnO nanopowders were synthesized by a conventional co-precipitation route and investigated with emphasis on their crystal structure, dielectric response and AC electrical conductivity. Powder X-ray diffraction (XRD) measurements showed the characteristic reflections of hexagonal wurtzite ZnO for the $Zn_{0.92}Fe_{0.08}O$ (Fe/ZnO-400) samples, with no additional crystalline reflections. Structural parameters obtained from the XRD analysis showed that the $Zn_{0.92}Fe_{0.08}O$ (Fe/ZnO-400) samples exhibited a crystallite size of approximately 38.5 nm. The corresponding interplanar spacing and unit-cell volume were calculated as 2.690 nm and 57.44 Å^3, respectively. To examine the electrical response of the Fe-modified ZnO samples, dielectric and AC conductivity measurements were carried out over a frequency range extending from 10 Hz to 5 MHz.

Keywords: ZnO; Fe doping; co-precipitation; X-ray diffraction; dielectric constant; AC conductivity.

1. INTRODUCTION

Metal-oxide nanomaterials exhibit structural, optical, and electrical properties that are strongly dependent on composition, crystallite size, defect chemistry, and microstructure. Zinc oxide (ZnO) is a widely investigated II–VI semiconductor because of its direct wide band gap, characteristic wurtzite crystal structure, and useful electrical and optoelectronic properties. These characteristics have motivated investigations of ZnO for sensing, photovoltaic, catalytic, actuator, and spintronic applications [1–4]. At ambient conditions, ZnO commonly adopts the hexagonal wurtzite structure described by the $P6_3mc$ space group.

The functional properties of ZnO can be modified through control of particle size, morphology, defect population, and chemical composition. In particular, incorporation of transition-metal ions into the ZnO lattice is of interest because dopants can alter local bonding, defect states, charge transport, and polarization processes [5–9]. Fe is especially relevant because Fe ions can interact with the ZnO host lattice and influence its structural and electrical behavior. Previous studies have therefore investigated Fe-doped ZnO prepared by different synthesis routes, including co-precipitation [7].

In the present work, Fe-modified ZnO was prepared by co-precipitation and subsequently annealed at 400 °C. The structural characteristics were examined by XRD, while the frequency dependence of the dielectric constant and AC conductivity was investigated at 310 K. Particular attention is given to the low-frequency polarization response and the frequency-dependent charge-transport behavior of the Fe/ZnO-400 sample.

2. EXPERIMENTAL DETAILS

2.1. Chemicals and synthesis procedure

Zinc acetate dihydrate [$Zn(CH_3COO)_2 \cdot 2H_2O$], sodium hydroxide (NaOH), iron nitrate nonahydrate [$Fe(NO_3)_3 \cdot 9H_2O$], ethanol (C_2H_5OH), and deionized (DI) water were used as starting materials. The required quantities of zinc acetate, iron nitrate, and sodium hydroxide were selected according to the target composition of the Fe-modified ZnO material. The precursor salts were dissolved in a suitable ethanol/DI-water mixture under continuous stirring. The resulting solution was stirred for approximately 2 h at 80 °C to promote homogeneous mixing and precipitation. The suspension was then kept undisturbed overnight. The precipitate was repeatedly washed with DI water to remove residual soluble species and subsequently dried in a vacuum oven at 90 °C for 12 h. The dried powder was finally annealed at 400 °C for 2 h. The annealed products were designated $Zn_{0.92}Fe_{0.08}O$ (Fe/ZnO-400).

© IARJSET This work is licensed under a Creative Commons Attribution 4.0 International License

IARJSET ISSN (O) 2393-8021, ISSN (P) 2394-1588

International Advanced Research Journal in Science, Engineering and Technology

Impact Factor 8.311 ⁜ Peer-reviewed & Refereed journal ⁜ Vol. 13, Issue 10, October 2026

DOI: 10.17148/IARJSET.2026.131039

2.2. Structural characterization

Powder XRD was used to identify the crystalline phase and to estimate the structural parameters. The diffraction patterns were recorded over 2θ = 10–80° using Cu Kα radiation (λ = 1.54 Å). The average crystallite size was estimated from the Scherrer equation:

$$D = K\lambda/(\beta \cos \theta) \quad \ldots\ldots\ldots\ldots\ldots\ldots\ldots\ldots(1)$$

where D is the mean crystallite size, K is the shape factor (taken as 0.91), λ is the X-ray wavelength, β is the FWHM of the selected diffraction peak expressed in radians after appropriate instrumental-broadening correction, and θ is the corresponding Bragg angle.

The interplanar spacing was calculated from Bragg's law:

$$2d \sin \theta = n\lambda \quad \ldots\ldots\ldots\ldots\ldots\ldots\ldots\ldots (2)$$

For the hexagonal ZnO structure, the lattice parameters were obtained from the indexed reflections using:

$$a = d_{hkl} * \sqrt{h^2 + k^2 + l^2} \quad \ldots\ldots\ldots\ldots\ldots\ldots (3)$$

$$V = (\sqrt{3}/2)\, a^2 c \quad \ldots\ldots\ldots\ldots\ldots\ldots\ldots\ldots (4)$$

2.3. Dielectric and AC conductivity measurements

The dielectric response was evaluated from the complex impedance measured as a function of frequency at 310 K. With Z′ and Z″ denoting the real and imaginary components of impedance, respectively, the real and imaginary parts of the relative permittivity were obtained from:

$$\varepsilon' = \frac{1}{\omega C_o}\left(\frac{Z''}{Z'^2 + Z''^2}\right) \quad \ldots\ldots\ldots\ldots\ldots\ldots(5)$$

$$\varepsilon'' = \frac{1}{\omega C_o}\left(\frac{Z'}{Z'^2 + Z''^2}\right) \quad \ldots\ldots\ldots\ldots\ldots\ldots(6)$$

where ω = 2πf is the angular frequency and C_0 is the geometrical capacitance of the empty measuring cell/pellet configuration.

The frequency-dependent AC conductivity was calculated using:

$$\sigma_{AC}(\omega) = \varepsilon_0\, \varepsilon'\, \omega \tan \delta \quad \ldots\ldots\ldots\ldots\ldots(7)$$

where ε_0 is the permittivity of free space.

3. RESULTS AND DISCUSSION

3.1. XRD analysis

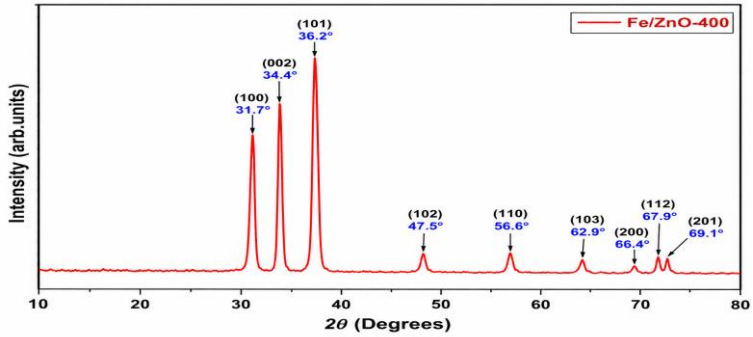


Figure 1. XRD patterns of $Zn_{0.92}Fe_{0.08}O$ (Fe/ZnO-400).

IARJSET ISSN (O) 2393-8021, ISSN (P) 2394-1588

International Advanced Research Journal in Science, Engineering and Technology

Impact Factor 8.311 ⁜ Peer-reviewed & Refereed journal ⁜ Vol. 13, Issue 10, October 2026

DOI: 10.17148/IARJSET.2026.131039

The XRD patterns exhibit diffraction reflections that correspond well with the standard JCPDS reference No. 80-0075, confirming the presence of the hexagonal wurtzite ZnO phase. The diffraction data were collected over a 2θ interval ranging from 10° to 80°. The major reflections are located near 31.7°, 34.4°, 36.2°, 47.5°, 56.6°, 62.9°, 66.4°, 67.9°, and 69.1°, corresponding to the (100), (002), (101), (102), (110), (103), (200), (112), and (201) planes, respectively. No additional well-resolved crystalline reflections are apparent in the supplied patterns, indicating that no secondary crystalline phase is detectable within the sensitivity of the XRD measurement. The absence of additional reflections supports retention of the ZnO wurtzite framework after Fe incorporation and annealing.

Table 1. Structural Analysis of $Zn_{0.92}Fe_{0.08}O$ (Fe/ZnO-400) nanoparticles.

Sample	Crystalline size (nm)	Inter planar spacing (d) Å	lattice constant Å		Volume (V) Å^3
			a=b	c	
$Zn_{0.92}Fe_{0.08}O$ (Fe/ZnO-400)	38.5	2.690	3.553	5.319	57.44

3.2. Dielectric constant

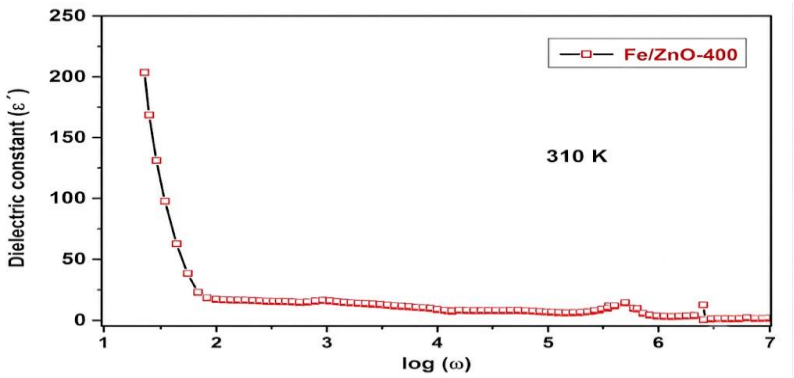


Figure 2 Frequency dependence of the real part of relative permittivity (ε′) for $Zn_{0.92}Fe_{0.08}O$ (Fe/ZnO-400) at 310 K.

The real part of the relative permittivity (ε′) of $Zn_{0.92}Fe_{0.08}O$ (Fe/ZnO-400) shows pronounced frequency dispersion at 310 K. The dielectric response is high at low frequency and decreases rapidly as frequency increases, followed by a much smaller variation at higher frequency. At low frequencies, charge carriers have sufficient time to migrate and accumulate at interfaces, grain boundaries, and other electrically heterogeneous regions. This charge accumulation can produce space-charge and interfacial polarization, thereby increasing the measured permittivity. As the frequency increases, the direction of the applied field changes more rapidly, reducing the distance over which mobile carriers can migrate and limiting their accumulation at interfaces. The residual variation at intermediate frequency may reflect localized relaxation processes associated with defects, grain boundaries, and other microstructural heterogeneities. At sufficiently high frequency, the slower polarization mechanisms cannot follow the alternating field effectively, so their contribution to ε′ becomes smaller. The observed dispersion is therefore qualitatively consistent with an electrically heterogeneous microstructure in which more conductive regions are separated by comparatively resistive interfaces, as commonly described using Maxwell–Wagner interfacial polarization and Koop-type phenomenological models [10–13].

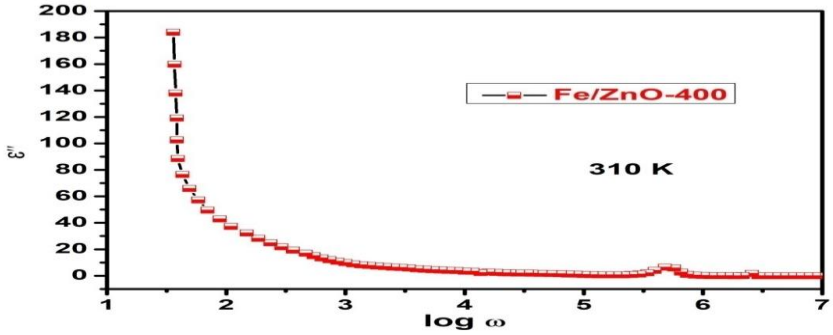


Figure 3. Frequency dependence of the imaginary part of relative permittivity (ε″) for $Zn_{0.92}Fe_{0.08}O$ (Fe/ZnO-400) at 310 K.

© IARJSET This work is licensed under a Creative Commons Attribution 4.0 International License

IARJSET ISSN (O) 2393-8021, ISSN (P) 2394-1588

International Advanced Research Journal in Science, Engineering and Technology

Impact Factor 8.311 ⁜ Peer-reviewed & Refereed journal ⁜ Vol. 13, Issue 10, October 2026

DOI: 10.17148/IARJSET.2026.131039

At low frequencies, ε′′ exhibits a considerably high value followed by a steep decline with increasing frequency. This behavior can be explained by the dominant contribution of slow polarization mechanisms, particularly the accumulation of charge carriers at grain boundaries, interfaces, and defect-associated regions. In the intermediate-frequency region, ε′′ shows only a gradual variation, suggesting that the influence of space-charge polarization becomes progressively weaker. At higher frequencies, ε′′ approaches a relatively low value because the localized charges and dipolar entities cannot reorient rapidly enough to remain synchronized with the applied field. Therefore, the frequency-dependent dielectric response of $Zn_{0.92}Fe_{0.08}O$ (Fe/ZnO-400) can be attributed to the combined effects of interfacial charge accumulation, grain-boundary polarization, structural defects, and localized charge-carrier relaxation [10-12]

3.3 AC conductivity

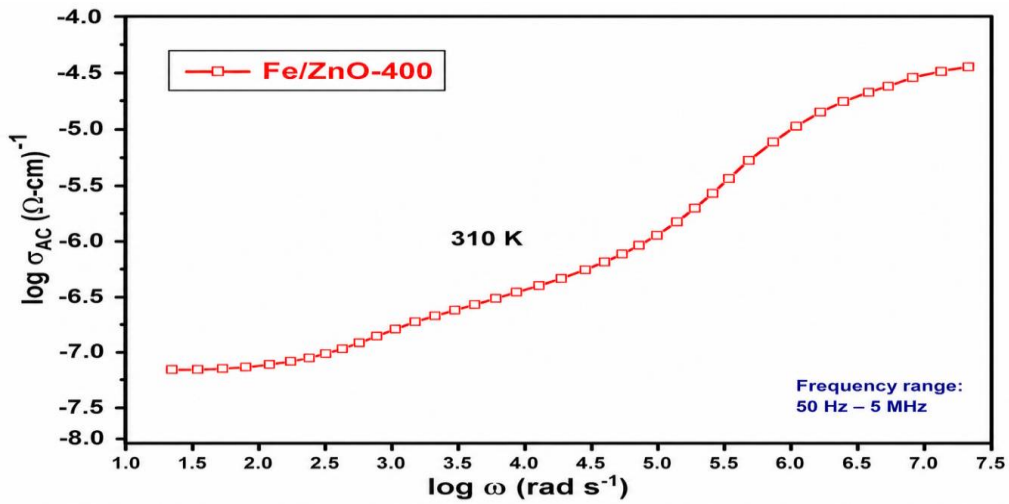


Figure 4. Frequency dependence of AC conductivity for $Zn_{0.92}Fe_{0.08}O$ (Fe/ZnO-400) at 310 K.

The AC conductivity of $Zn_{0.92}Fe_{0.08}O$ (Fe/ZnO-400) increases progressively with increasing frequency at 310 K. The low-frequency portion shows a comparatively weak frequency dependence, followed by a stronger dispersive increase at higher frequencies. A low-frequency plateau, when clearly resolved, is commonly associated with the frequency-independent DC contribution, whereas the subsequent dispersive region reflects AC charge transport. The increase in conductivity with frequency can be associated with localized charge-carrier motion and hopping between energetically accessible sites. In a structurally heterogeneous oxide, grain interiors and grain boundaries can possess different electrical resistivities, producing frequency-dependent charge accumulation and transport. The observed behavior is therefore qualitatively compatible with the Koop/Maxwell–Wagner framework used to describe heterogeneous dielectric materials [10-12]. The conductivity log σ(ω) for $Zn_{0.92}Fe_{0.08}O$ (Fe/ZnO-400) at 300 k is obtained -7.158 $(\Omega\text{-cm})^{-1}$.

4. CONCLUSION

Fe-modified ZnO nanostructures were synthesized by co-precipitation and investigated after annealing at 400 °C. XRD analysis showed that $Zn_{0.92}Fe_{0.08}O$ (Fe/ZnO-400) retains the characteristic hexagonal wurtzite ZnO structure, with no additional well-resolved crystalline phase in the supplied diffraction patterns. The dielectric measurements of $Zn_{0.92}Fe_{0.08}O$ (Fe/ZnO-400) at 310 K shows strong low-frequency dispersion in ε′ and ε″. These features are consistent with interfacial and space-charge polarization at low frequencies and reduced response of slow charge carriers at higher frequencies. The conductivity log σ(ω) for $Zn_{0.92}Fe_{0.08}O$ (Fe/ZnO-400) at 300 k is obtained -7.158 $(\Omega\text{-cm})^{-1}$. The AC conductivity increases with frequency, indicating frequency-dependent localized charge transport.

REFERENCES

[1]. B. Sharma et al., “Synthesis and characterization of polyaniline–ZnO composite and its dielectric behavior,” Synthetic Metals 159 (2009) 391–395.

[2]. D. Gao et al., “Room temperature ferromagnetism of pure ZnO nanoparticles,” Journal of Applied Physics 105 (2009) 113928.

DOI: 10.17148/IARJSET.2026.131039

[3]. T. Sahoo et al., "Synthesis and characterization of porous ZnO nanoparticles by hydrothermal treatment of as pure aqueous precursor," Materials Research Bulletin 46 (2011) 525–530.

[4]. S. B. Rana et al., "Synthesis and characterization of pure and doped ZnO nanoparticles," Journal of Optoelectronics and Advanced Materials 12 (2010) 257.

[5]. S. Muthukumaran and R. Gopalakrishnan, "Structural, FTIR and photoluminescence studies of Cu doped ZnO nanopowders by co-precipitation method," Optical Materials 34 (2012) 1946–1953.

[6]. J. Husain et al., "Electrical properties of polyaniline/Cadmium Oxide/ZnO Nanocomposites Thin Films," International Research Journal on Advanced Science Hub 2 (2020) 31–33. https://doi.org/10.47392/irjash.2020.89.

[7]. K. Raja et al., "Structural, FTIR and photoluminescence studies of Fe doped ZnO nanopowder by co-precipitation method," Spectrochimica Acta Part A: Molecular and Biomolecular Spectroscopy 131 (2014) 183–188.

[8]. R. S. K. Rashmi, H. S. Bhojya Naik, and H. Jayadevappa, "Optical and photocatalytic application of ZnFe2O4–SmFeO3 nanocomposites," International Research Journal on Advanced Science Hub 2 (2020) 123–130. https://doi.org/10.47392/irjash.2020.105.

[9]. F. Ahmed et al., "Doping effects of Co2+ ions on structural and magnetic properties of ZnO nanoparticles," Acta Materialia 60 (2012) 5190–5196.

[10]. D. Mohapatra et al., "High performance flexible asymmetric CNO-ZnO//ZnO supercapacitor with an operating voltage of 1.8 V in aqueous medium," Applied Materials Today 7 (2017) 212–221.

[11]. P. Anandhi et al., "Improved electrochemical behavior of metal oxides-based nanocomposites for supercapacitor," Functional Materials Letters 12 (2019) 1950064.

[12]. L. Wang et al., "Recent progress in Zn-based anodes for advanced lithium ion batteries," Materials Chemistry Frontiers 2 (2018) 1414–1435.

[13]. B. Zhu et al., "Interfacial stabilizing effect of ZnO on Si anodes for lithium ion battery," Nano Energy 13 (2015) 620–625.

© IARJSET This work is licensed under a Creative Commons Attribution 4.0 International License